TWO-PHASE PAIR CORONA MODEL FOR AGN: PHYSICAL MODELLING AND DIAGNOSTICS

Juri Poutanen[1,2]**, Roland Svensson**[1]**, and Boris Stern**[1,3]

[1]Stockholm Observatory, Saltsjöbaden, Sweden

[2]Uppsala Astronomical Observatory, Uppsala, Sweden

[3]Institute for Nuclear Research, Moscow, Russia

ABSTRACT

The predictions of the two-phase accretion disc-corona models for active galactic nuclei are compared with observations. We discuss the possibility to use X-ray spectral slopes, equivalent widths of the iron line, and the observed flux-spectral index correlation as diagnostics of the X-γ-ray source compactness and geometry as well as of the cold disc temperature. As an example of the application of the modelling tools, we use XSPEC to fit the broad-band data of Seyfert 1 galaxy, IC4329A, with a theoretical spectrum from a hemisphere-corona.

Keywords: accretion, accretion discs; galaxies: Seyfert; gamma rays: theory; X-rays: galaxies.

1. INTRODUCTION

Observations of Seyfert 1 galaxies by *Ginga* and earlier by *HEAO 1* showed that their X-ray spectra consist of at least two distinct components: an intrinsic power-law with energy index, α_{2-18} =0.95±0.15, in 2 - 18 keV range and a Compton reflection bump (Mushotzky, Done, & Pounds 1993, Nandra & Pounds 1994, Weaver et al. 1995). Recent *ASCA* observations also show these features (Nandra et al. 1996). *OSSE* observations show a much steeper spectrum with $\alpha \approx 1.5$ (Johnson et al. 1996), and *COMP-TEL* has not detected Seyfert galaxies at all (Maisack et al. 1995). Averaged broad-band spectrum for a sample of Seyfert 1 galaxies which was obtained using non-simultaneous *Ginga* and OSSE data shows a high-energy cutoff of the intrinsic power-law at E_c =600$^{+800}_{-300}$ keV (Zdziarski et al. 1995). A similar cutoff energy is obtained by Gondek et al. (1996) using the data from *EXOSAT* and OSSE. *ROSAT, Ginga* and OSSE data of the Seyfert 1 galaxy, IC4329A, also require a cutoff in the intrinsic spectrum (Madejski et al. 1995). The brightest Seyfert galaxy in γ-rays, NGC 4151, shows a cutoff at $\sim$ 150 keV, but is probably a freak object requiring special considerations (Poutanen et al. 1996, but see Zdziarski et al. 1997).

Non-thermal pair models intensively studied in the mid 80s (Svensson 1986, for review see Svensson 1994) predicted the spectral index of the intrinsic component $\alpha_{\rm int} \approx 0.9 - 1.0$ and a prominent pair annihilation line. Absence of the annihilation line in the observed spectra rules out pure non-thermal models. Attention is now focused on thermal models. A definite answer on the question about the relative fraction of the thermal and non-thermal plasma cannot be obtained without high quality data above 200 keV.
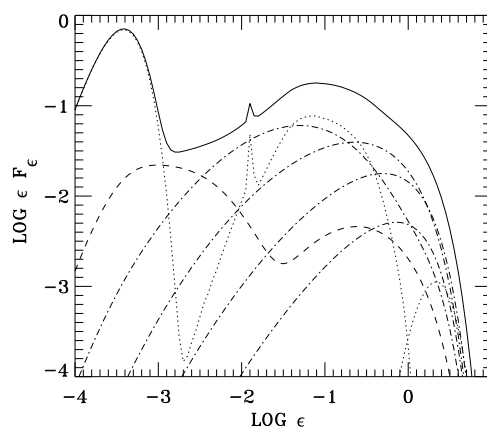

Figure 1: *An example of the deconvolution of the emergent spectrum from a disc-corona system into different scattering orders. Solid curve represents the total emergent spectrum. Dotted curves give the contribution of the unscattered radiation which consists of three components: black-body radiation with a maximum at $\epsilon \equiv h\nu/m_e c^2 \approx 3{\cdot}10^{-4}$, a Compton reflection component with a maximum at $\epsilon \approx 0.1$, and a broad annihilation line at $\epsilon \approx 2$. Dashed curve gives the contribution of the single scattered radiation (notice that the broad bump with a maximum at $\epsilon \approx 0.2$ is the first scattering order of the Compton reflection component). All other scattering orders are represented by dash-dotted curves.*

There is a consensus that the X/γ-ray spectrum of Seyferts is produced by Comptonization in hot plasmas of soft radiation from the UV source. The exact geometry of both phases is unknown. Presently, the most commonly used scenario is the two-phase disc-corona model (e.g., Haardt & Maraschi 1991, 1993) in which a hot X-ray emitting corona is located above the cold UV-emitting disc of the canonical black hole

model for AGNs. The power-law X-ray spectrum is generated by thermal Comptonization of the soft UV-radiation. About half of the X-rays enters and is reprocessed by the cold disc, emerging mostly as black body disc radiation in the UV (some fraction is reflected producing a Compton reflection component). Haardt & Maraschi (1991) emphasized the coupling between the two phases due to the reprocessing, as the soft disc photons influence the cooling of the corona. They showed that nearly all power must be dissipated in the corona in order to have $\alpha_{\rm int} \sim$ 0.9-1. A consequence of this is that the soft disc luminosity, L_s, is of the same order as the hard X-ray luminosity, L_h.
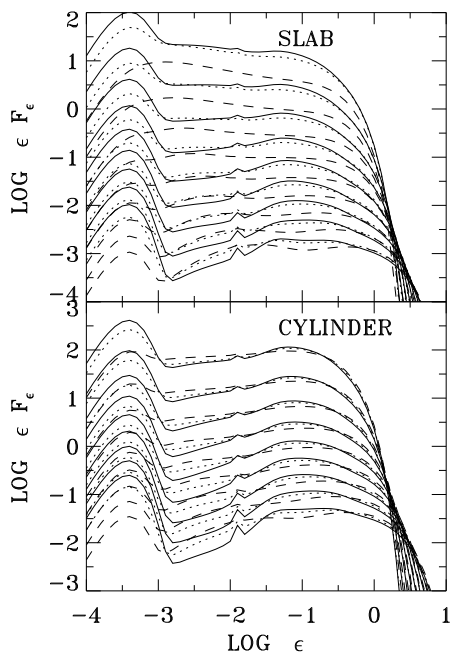

Figure 2: Upper panel: spectra emerging in different directions from a slab-corona. Solid, dotted, and dashed curves represent the flux at viewing cosine angle μ=0.9, 0.5 and 0.1, respectively. The temperature of the blackbody radiation from the accretion disc is fixed at $T_{\rm bb}$=50 eV. The electron temperature of the corona increases from the top of the figure to the bottom: $\Theta \equiv kT_{\rm e}/mc^2$= 0.16, 0.2, 0.25, 0.32, 0.4, 0.5, 0.63, 0.79, 1.0. Notice the increase of the iron line equivalent width with increasing temperature due to anisotropic scattering effects (see, e.g., Haardt & Maraschi 1993, Stern et al. 1995b). The iron line profile has a triangular shape due to the energy resolution employed here. Lower panel: spectra from a cylinder-corona with a height-to-radius ratio 2.

Observations show that L_s may be several times larger than L_h, in contradiction to the prediction of the uniform two-phase disc-corona model. This led Haardt, Maraschi, & Ghisellini (1994) to propose a patchy disc-corona model, where the corona consists of several localized active regions on the surface of the disc. Internal disc dissipation results in UV-radiation that leaves the disc without entering the active regions, thus enhancing the observed L_s relative to L_h.

The first exact radiative transfer/Comptonization calculations in a disc-corona system accounting for energy and pair balance as well as reprocessing by the cold disc (including angular anisotropy) were re-

ported in Stern et al. 1995b. Two methods were used. The first method is based on the Non-Linear Monte-Carlo method by Stern (see detailed description in Stern et al. 1995a). The second method is the iterative scattering method (ISM) where the radiative transfer is exactly solved for each scattering order separately (Poutanen & Svensson 1996). The results of both codes are in excellent agreement. In this paper we report the results using the second method. A typical spectrum emerging from the disc-corona system and its different components is shown in Figure 1.

2. SPECTRA FROM THE DISC-CORONA SYSTEM

The ISM code is a 1D code but it can also treat quasi-2D radiative transfer in cylinders and hemispheres. The full Compton scattering matrix is used allowing us to treat polarized radiative transfer in thermal relativistic plasmas. Fully angular dependent, polarized Compton reflection is implemented using a Green's matrix (Poutanen, Nagendra, & Svensson 1996). For a given geometry, energy balance gives a unique combination of electron temperature $\Theta = kT_{\rm e}/m_e c^2$ and Thomson optical depth, $\tau_{\rm T} = n_e\sigma_{\rm T}h$. Solving the pair balance for a given (Θ, $\tau_{\rm T}$) provides a unique dissipation compactness, $l_{\rm diss}$ (Ghisellini & Haardt 1994). Here, the local dissipation compactness, $l_{\rm diss} \equiv (L_{\rm diss}/h)(\sigma_{\rm T}/m_e c^3)$, characterizes the dissipation with $L_{\rm diss}$ being the power providing uniform heating in a cubic volume of size h in the case of a slab of height h, or in the whole volume in the case of an active region (cylinder or hemisphere) of height h. The relation between Θ, $\tau_{\rm T}$, and $l_{\rm diss}$ for different geometries is given in Stern et al. (1995b) (see also Svensson 1996).

Figure 2 shows spectra from slab-corona and cylinder-corona at different Θ. As the temperature increases the first order scattered photons are predominantly scattered back into the disc, causing a deficiency of the first order photons in the observed spectrum. This anisotropic effect gives rise to an anisotropy break in the spectra (Stern et al. 1995b).

3. DIAGNOSTICS USING SPECTRAL SLOPES AND IRON LINE EQUIVALENT WIDTHS

In order to compare the predictions of the two-phase corona model with observations, we determine the least square overall spectral slope, α_{2-18}, for theoretical model spectra and display them in Figure 3 as a function of the dissipation compactness, $l_{\rm diss}$, for different geometries. The right panels show the observed distributions of the spectral indices for *Ginga* spectra of 27 Seyfert galaxies (Nandra & Pounds 1994) and for *ASCA* spectra (2 - 10 keV range) of 15 Seyfert 1s (Nandra et al. 1996). One sees that the observations are more consistent with active surface regions (such as hemispheres or cylinders) than with slabs. Active regions produce spectra covering the *observed ranges* of spectral indices and cutoff energies for the *observed range* of compactnesses.

For small temperature of the black-body, T_{bb}, anisotropic effects significantly change the spectral index at compactnesses smaller than ~ 100. For $T_{bb}=50$ eV, the anisotropy break in the 2 - 18 keV range appears all the way up to $l_{diss} \approx 1000$. For such a high temperature of the soft radiation, the first scattering order extends up to the *Ginga* range already for $T_e \approx 100$ keV.

When the anisotropy break shifts to the spectral region around the fluorescent iron line at 6.4 keV, the continuum flux in the direction of the cold disc exceeds the flux in the observer's direction, causing an increase of the equivalent width of the K-line in comparison with the isotropic case. This effect is demonstrated in Figure 4 where the iron line equivalent width is plotted against the electron temperature for different geometries. We also show the distribution of the equivalent widths observed by *ASCA* (Nandra et al. 1996).
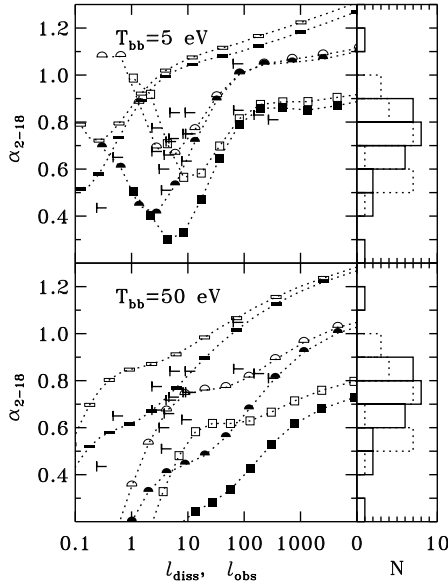
Figure 4: *Equivalent width of the iron K-line at 6.4 keV vs. electron temperature, Θ. Same notations as in Figure 3. Notice that for low temperature, the equivalent width is almost constant. It increases when the temperature increases due to the anisotropy effects (see Fig. 2). For higher disc temperature, T_{bb}, the anisotropy effects become important at smaller electron temperature. Right panels show the distribution of the equivalent widths of Seyfert 1s observed by ASCA (Nandra et al. 1996, Table 6).*

Figure 3: *Overall power-law index, α_{2-18}, least-square fitted to the model spectra in the 2 - 18 keV energy range vs. dissipation compactness, $l_{diss} \equiv (L_{diss}/h)(\sigma_T/m_e c^3)$. Rectangles, hemispheres, and squares represent results for the slab-corona, hemisphere-corona, and cylinder-corona (with height-to-radius ratio 2), respectively. Filled symbols correspond to the spectra in almost face-on direction ($\mu=0.9$), open symbols represent results for inclination $60°$ ($\mu=0.5$). Results for $T_{bb}=5$ eV and $T_{bb}=50$ eV are presented in upper and lower panels, respectively. Lower compactness limits represent Seyfert galaxies that have known estimates of their X-ray variability, Δt, and thus lower limits of their compactnesses, $l_{obs} \equiv (L_{obs}/c\Delta t)(\sigma_T/m_e c^3)$, see Done & Fabian 1989. The right panels shows the observed distributions of power-law indices of Seyfert galaxies. Solid histogram: Ginga data from Nandra & Pounds (1994). Dotted histogram: ASCA data from Nandra et al. (1996, Table 2).*
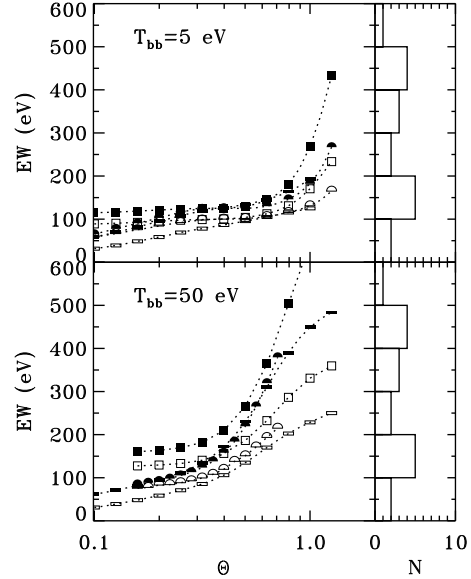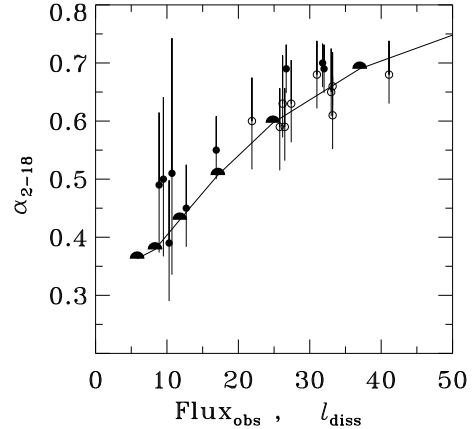
Figure 5: *Correlation between spectral index, α_{2-18}, and the continuum flux in 2 - 10 keV energy band corrected for absorption (in units of 10^{-11} erg s^{-1} cm^{-2}) observed by Ginga in NGC 4151. Filled spheres with the error bars show the data from Yaqoob & Warwick (1991) and open spheres are the data from Yaqoob et al. (1993). Hemispheres and solid curve show the correlation between spectral index and dissipation compactness (arbitrary compactness units) for the hemisphere-corona model. Similar correlation is expected also in non-thermal pair models (see Yaqoob 1992).*

4. FLUX - SPECTRAL INDEX CORRELATION

Some Seyfert galaxies show correlated variations in flux and spectral index (see, e.g., Matsuoka et al. 1990, Treves et al. 1990, Yaqoob & Warwick 1991, Yaqoob et al. 1993). This correlation has been explained in the context of non-thermal pair model (e.g. Yaqoob 1992). Our thermal pair model shows strong correlation between compactness parameter and the spectral index (see Fig. 3). Assuming that the size of the X/γ source is constant there is a direct correspondence between l_{diss} and the observed flux (here we neglect the effect of spectral changes with compactness). Figure 5 shows the flux – spectral index correlation observed in NGC 4151 and the compactness – spectral index correlation for a hemisphere-corona (l_{diss} is in arbitrary units and is rescaled to fit observations). It can be seen in Figure 3, that for T_{bb}=5 eV spectral index changes dramatically from 1.0 to 0.5 when l_{diss} changes by an order of magnitude from 100 to 10.

5. SPECTRAL FITTING

We implemented the ISM code into XSPEC, and used it to fit the broad band spectrum of the second brightest Seyfert 1 galaxy, IC4329A. As an example, we fitted data with theoretical spectra from a hemisphere-corona. The spectrum is absorbed by a combination of neutral and ionized absorbers. It is presently difficult to constrain the temperature of the black-body radiation, T_{bb}, and hence we fixed it at 10 eV. The best fit model parameters are T_{e}=100$^{+10}_{-30}$ keV, and τ_{T}=1.3$^{+0.4}_{-0.2}$. The quality of the data does not allow us to constrain the geometry of the emitting region. The data and the model spectrum are shown in Figure 6.
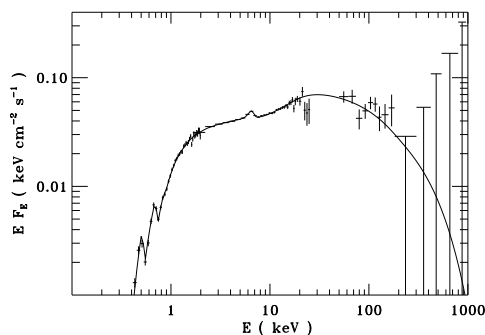

Figure 6: *The broad-band spectrum of Seyfert 1 galaxy, IC4329A. ROSAT, Ginga, and OSSE observations are described in Madejski et al. (1995). The upper limits are 2σ. Solid curve shows the best fit hemisphere-corona model spectrum.*

6. CONCLUSIONS

Several diagnostics from physical modelling of observed spectra are possible. (1) As anisotropic effects are very important, i.e. as spectral shapes depend strongly on viewing angle, it will be possible to set constraints on the viewing angle within the framework of the two-phase pair corona model, once high quality spectra become available. (2) The spectra also depend on the geometry of the coronal regions, so observed high quality spectra can be used as diagnostics of the geometry. Presently, it seems that active regions are favored over homogeneous slab coronae. (3) Observations of flux-index correlations can provide constraints on the source compactness. (4) The equivalent width of the iron line can be used as a diagnostic of the temperature of the reprocessed (black-body) radiation which then constrains the size.

REFERENCES

Done, C., Fabian, A. C. 1989, MNRAS, 240, 81

Johnson, W. N., et al. 1996, A&AS, in press

Ghisellini, G., Haardt, F. 1994, ApJ, 429, L53

Gondek, D., et al. 1996, MNRAS, 282, 646

Haardt, F., Maraschi, L. 1991, ApJ, 380, L51

Haardt, F., Maraschi, L. 1993, ApJ, 413, 507

Haardt, F., Maraschi, L., Ghisellini, G. 1994, ApJ, 432, L95

Madejski, G. M., et al. 1995, ApJ, 438, 672

Maisack, M., et al. 1995, A&A, 298, 400

Matsuoka, M., Piro, M., Yamauchi, M., Murakami, T. 1990, ApJ, 361, 440

Mushotzky, R. F., Done, C., Pounds, K. A. 1993, ARA&A, 31, 717

Nandra, K., Pounds, K. A. 1994, MNRAS, 268, 405

Nandra, K., George, I. M., Mushotzky, R. F., Turner, T. J., Yaqoob, T. 1996, ApJ, in press

Poutanen, J., Nagendra, K. N., Svensson, R. 1996, MNRAS, in press

Poutanen, J., Sikora, M., Begelman, M. C., Magdziarz, P. 1996, ApJ, 465, L107

Poutanen, J., Svensson, R. 1996, ApJ, 470, 249

Stern, B. E., Begelman, M. C., Sikora, M., Svensson, R., 1995a, MNRAS, 272, 291

Stern, B. E., Poutanen, J., Svensson, R., Sikora, M., Begelman, M. C. 1995b, ApJ, 449, L13

Svensson, R. 1986, in D. Mihalas, K-H. Winkler (eds.), Radiation Hydrodynamics in Stars and Compact Objects, Vol. 89 of *IAU Colloquium*, Springer, New York

Svensson, R. 1994, ApJS, 92, 585

Svensson, R. 1996, A&AS, in press

Treves, A., et al. 1990, ApJ, 359, 98

Weaver, K. A., Arnaud, K. A., Mushotzky, R. F. 1995, ApJ, 447, 121

Yaqoob, T. 1992, MNRAS, 258, 198

Yaqoob, T., Warwick, R. S. 1991, MNRAS, 248, 773

Yaqoob, T., Warwick, R. S., Makino, F., Otani, C., Sokoloski, J. L., Bond, I. A., Yamauchi, M. 1993, MNRAS, 262, 435

Zdziarski, A. A., Johnson, W. N., Done, C., Smith, D., McNaron-Brown, K. 1995, ApJ, 438, L63

Zdziarski, A. A., Johnson, W. N., Poutanen, J., Magdziarz, P., Gierlinski, M. 1997, these proceedings